Ocean Engineering 178 (2019) 484–492

Contents lists available at ScienceDirect

Ocean Engineering

journal homepage: www.elsevier.com/locate/oceaneng

Compensation of bias loads in dynamic positioning of marine surface vessels

Svenn A. Værnø*, Astrid H. Brodtkorb, Roger Skjetne

Department of Marine Technology, Norwegian University of Science and Technology, 7052, Trondheim, Norway

ARTICLE INFO

Keywords:
Dynamic positioning
Control design
Observers
Integral control

ABSTRACT

This paper investigates different methods for compensating the mean and slowly varying environmental loads, and unmodeled dynamics (bias loads) in dynamic positioning of marine vessels. Four different methods are compared; using the bias estimate from an observer tuned to estimate position and velocity well, using a wave-filtered version of this bias load, using the estimate from a separate observer tuned to work well for estimating the bias loads, and finally traditional integral action on the tracking errors. The results show that the bias from the bias observer is the best solution, both in transients and steady state. Standard integral action matches the steady state performance, but is slower in transients. The estimate from the observer used for position and velocity is fast in transients, but too oscillatory in the bias state. The wave-filtered version of this has less oscillations, but falls short compared to the other methods due to added phase lag from the extra wave filter. Using a bias estimate from an observer has benefits over typical integral action, such as the possibility of offline or open-loop tuning and avoiding integral windup issues. For the comparison study, a 6 DOF simulation model of a supply vessel is used.

1. Introduction

In control systems for dynamic positioning (DP) of marine vessels it is common to include integral action to compensate for the mean and slowly varying environmental disturbances and unmodeled dynamics. When using a model-based observer, the sum of the environmental disturbances and unmodeled dynamics is estimated in what is typically called a bias load (Fossen and Strand, 1999). Use of this bias load estimate in feedback instead of integral action has been proposed by Loria et al. (2000). However, for output feedback designs it is common in the literature (Sørensen, 2011) to include integral action in the controller even though this load is estimated in the observer. One reason for this could be the assumption that the bias estimate from the observer is too oscillatory to give good performance when used in feedback. Integral action is therefore introduced and tuned such that it is slow, calm (small oscillations), and works well in steady state.

Recently, however, there have been much focus on DP during transient conditions, e.g. due to sudden large wave trains, ice loads, frequent setpoint changes, etc., and the question has been asked if a slow integral action is suitable. As seen for instance in Refsnes and Sørensen (2007), Værnø et al. (2016), Værnø et al. (2017), Kjerstad and Skjetne (2016), Lindegaard (2003), and as discussed in Brodtkorb et al. (2016) and in Brodtkorb et al. (2018), the bias load can vary rapidly, even for common situations such as heading changes. In these instances, effective compensation of the bias load is beneficial. In the following we compare four different approaches for compensating the bias loads, with special focus on transient events. This problem received some attention by Værnø et al. (2016), but here the discussion is more rigorous.

A typical DP system is evaluated through numerical studies and model-scale experiments in Tannuri and Morishita (2006), and a model-based Kalman filter is presented for DP by Fossen and Perez (2009), initially proposed by Balchen et al. (1976). A robust controller presented by Du et al. (2015) uses a high-gain observer, in addition to neural networks to compensate for the unknown environmental disturbances. Typically, fault tolerance and robustness are system design properties that are considered (Blanke et al., 2003). For an overview of the DP system and a historical overview, see Sørensen (2011) and the references therein.

In this paper we refer to the bias compensation by a term $\hat{b}$ in the control law, where $\hat{b}$ is the estimated bias in an observer. Integral action, on the other hand, refers to an integral term ζ in the control law with $\dot{\zeta} = \hat{\eta} - \eta_d(t)$, that is, it integrates the tracking error based on the estimated vessel state $\hat{\eta}$.

Using the bias estimate from a model-based observer instead of typical integral action on the output tracking errors has some benefits. First, if we use the bias estimate from an observer instead of integral action, windup issues in the integrator are of no concern. However, it

* Corresponding author.
E-mail addresses: svenn.are.varno@ntnu.no (S.A. Værnø), astrid.h.brodtkorb@ntnu.no (A.H. Brodtkorb), roger.skjetne@ntnu.no (R. Skjetne).

https://doi.org/10.1016/j.oceaneng.2019.03.010
Received 14 June 2018; Received in revised form 19 January 2019; Accepted 4 March 2019
Available online 18 March 2019
0029-8018/

should be noted that if a separate observer is added to estimate the bias load, this adds similar complexity as an anti-windup filter in the controller (Perez, 2009). Another benefit of using a bias estimate from an observer is tuning. It is easier to tune an observer since you only need offline data series. In addition you can use optimization methods to find satisfactory gains. An advantage of using the integral action is that it can be tuned independently of the bias response time. This means, for instance, that the integral action can be tuned slow to account for steady-state offsets, whereas the bias estimate in the observer can be made faster and letting it live its own life. This tuning separation also applies if there is a separate observer to estimate the bias load.

The main contribution of this paper is an in-depth study into several best practices of compensating the unknown environmental loads and unmodeled dynamics for DP of marine vessels. The analysis of performance is made fair by the use of optimization in tuning of all observers, and also a thorough tuning of controller and integral action. The results are demonstrated through a high-fidelity simulation study. To the authors' knowledge, such a comparison does not exist in the literature. This study is important, as it allows for research-based design choices to be made when developing DP control systems.

Notation and terminology: A column vector is stated as $\text{col}(x, y, z) := [x^\top, y^\top, z^\top]^\top$, $\mathbb{R}_{>0}$ denotes positive real numbers, and $\mathbb{S}$ represents the angle defined on the interval $[-\pi, \pi)$.

2. Problem formulation

There are two reference frames typically used for DP; the North-East-Down (NED)-frame and body-frame. For operations in confined areas (such as DP) the NED-frame can be assumed to be a non-rotating global and inertial frame. This is a tangent plane to the Earth, with the x-axis pointing North, y-axis pointing East, and z-axis pointing down to the center of the Earth. The body-frame is a local frame with origin typically midships, in the centerline, and waterline of the vessel, with the x-axis pointing to the bow, y-axis to starboard, and z-axis down.

We separate between a *simulation verification model (SVM)* and a *control design model (CDM)*. The SVM is intended for observer and controller verification, and is a high-fidelity model. The CDM includes the dynamics that is most important for the operation. For low-speed application such as DP, this typically implies that the Coriolis, centripetal, and nonlinear damping loads are omitted from the model. As shown by Værnø et al. (2019), including nonlinear damping gives a slight improvement. However, because the improvement is not significant, and because it is not important for this study, it is not included in the CDM of this paper.

2.1. Control design model

We consider the 3 degrees of freedom (DOF) CDM (Fossen, 2011),

$$\dot{\xi} = A_w \xi + E_w w_w \tag{1a}$$

$$\dot{\eta} = R(\psi)\nu \tag{1b}$$

$$\dot{b} = w_b \tag{1c}$$

$$M\dot{\nu} = -D\nu + R(\psi)^\top b + \tau + \tau_{wind} \tag{1d}$$

$$y = \eta + C_w \xi + v_y, \tag{1e}$$

where $\xi \in \mathbb{R}^6$ in (1a) is the first order wave-induced dynamics of the vessel, and (1b)-(1d) is the low-frequency vessel dynamics. The first-order wave-induced dynamics makes the vessel oscillate about the setpoint at the wave frequency. Compensating this oscillatory motion causes extra wear and tear on the thrusters, and it is often not possible due to thruster limitations. For both of these reasons, we separate between the low-frequency and wave-frequency dynamics. The wave-frequency dynamics ξ in (1a) are modeled by a mass-spring-damper dynamics, where A_w is a Hurwitz matrix that contains the damping ratio and the peak frequency of the incident waves, and $w_w \in \mathbb{R}^6$ is white noise (Sørensen, 2013). The vector $\eta := \text{col}(\eta_N, \eta_E, \psi) \in \mathbb{R}^2 \times \mathbb{S}$ in (1b) contains the low-frequency North/East position, and heading, respectively, and $\nu := \text{col}(u, v, r) \in \mathbb{R}^3$ is the surge/sway velocity in the body-frame, and the yaw rate, respectively. The rotation matrix $R(\psi)$ rotates a 3 DOF vector from the body to the NED-frame according to

$$R(\psi) = \begin{bmatrix} \cos(\psi) & -\sin(\psi) & 0 \\ \sin(\psi) & \cos(\psi) & 0 \\ 0 & 0 & 1 \end{bmatrix}. \tag{2}$$

$\tau := \text{col}(\tau_{surge}, \tau_{sway}, \tau_{yaw}) \in \mathbb{R}^3$ is the generalized control vector in the body-frame, $\tau_{wind} \in \mathbb{R}^3$ is the wind load, which is measured, and $b := \text{col}(b_N, b_E, b_\psi) \in \mathbb{R}^3$ is the bias load vector, and $w_b \in \mathbb{R}^3$ is white noise. The vector b constitutes the sum of the low-frequency loads, such as the slowly-varying second-order wave loads, current loads, and unmodeled dynamics from errors in the mass, added mass, hydrodynamic damping, wind loads, and thrust mappings. The bias load vector is assumed constant (or slowly-varying) in the NED-frame. Finally, the measurement vector y is the sum of low-frequency North/East position and heading η, the wave-frequency North/East position and heading $C_w\xi$, where $C_\omega = [0_{3\times3} \;\; I_{3\times3}]$, and the measurement noise $v_y \in \mathbb{R}^3$.

2.2. Model-based observer

To estimate the low-frequency position η, velocity ν, and the bias b, a nonlinear observer (NLO) similar to the observer proposed by Fossen and Strand (1999) is chosen. The observer is given by

$$\dot{\hat{\xi}} = A_w \hat{\xi} + K_1 \tilde{y} \tag{3a}$$

$$\dot{\hat{\eta}} = R(\psi)\hat{\nu} + K_2 \tilde{y} \tag{3b}$$

$$\dot{\hat{b}} = K_3 \tilde{y} \tag{3c}$$

$$M\dot{\hat{\nu}} = -D\hat{\nu} + R(\psi)^\top \hat{b} + \tau + \tau_{wind} + K_4 R(\psi)^\top \tilde{y} \tag{3d}$$

$$\hat{y} = \hat{\eta} + C_w \hat{\xi}, \tag{3e}$$

where $\hat{\xi} \in \mathbb{R}^6$, $\hat{\eta} \in \mathbb{R}^2 \times \mathbb{S}$, $\hat{b} \in \mathbb{R}^3$, and $\hat{\nu} \in \mathbb{R}^3$ are the state estimates. The injection gains $K_1 = [K_{11}^\top \;\; K_{12}^\top]^\top \in \mathbb{R}^{6\times3}$, $K_2, K_3, K_4 \in \mathbb{R}^{3\times3}$ are non-negative matrices, and $\tilde{y} = y - \hat{y}$ is the measurement error. The matrices K_3 and K_4 are constant, whereas K_1 and K_2 depend on the peak frequency of the wave spectrum to obtain good wave-filtering. As in (Fossen and Strand, 1999) and many later references, we assume that:

(A1) $R(\psi^m) \approx R(\psi + \psi_w) \approx R(\psi)$. First, because of the low noise on the compass, we assume that the measured heading angle ψ^m is close to the real heading angle, that is, the sum of the low-frequency heading ψ and the wave-frequency heading ψ_w. Second, the heading angle due to wave-induced motion, ψ_w is small (negligible effect on the rotation matrix).

The assumption is justified because the wave-induced heading angle is typically less than 1° for normal sea states, and less than 5° for extreme sea states. Thus, the measured heading angle is used instead of the low-frequency heading angle in the rotation matrix.

2.3. Controller

The controller τ is given by a feedback part τ_{FB} and a reference feedforward part τ_{FF},

$$\tau = \tau_{FB} + \tau_{FF} \tag{4a}$$

$$\tau_{FF} = D\nu_d(t) + M\dot{\nu}_d(t) - \tau_{wind} \tag{4b}$$

$$\tau_{FB} = \tau_{nPD} + \tau_{BR}, \tag{4c}$$

where τ_{nPD} is a nonlinear proportional-derivative (nPD) controller given by

$$\tau_{nPD} = -K_p R(\psi)^\top(\hat{\eta} - \eta_d(t)) - K_d(\hat{\nu} - \nu_d(t)), \tag{4d}$$

and $\eta_d \in \mathbb{R}^2 \times \mathbb{S}$, $\nu_d \in \mathbb{R}^3$, and $\dot{\nu}_d(t) \in \mathbb{R}^3$ are bounded references generated by a guidance system, $K_p \in \mathbb{R}^{3\times3}$ and $K_d \in \mathbb{R}^{3\times3}$ are positive definite gain matrices, and τ_{BR} is a bias rejection term to compensate for $R(\psi)^\top b$ in (1d). Designs for τ_{BR} is the main focus of this paper and will be elaborated in Section 2.4.

2.4. Methods for bias compensation

In the following, four methods for compensating the bias load, τ_{BR} in (4c), are presented:

- Method 1: Direct compensation
- Method 2: Wave-filtered bias estimate
- Method 3: Separate bias observer
- Method 4: Integral action.

All the methods use estimates of η and ν from the same observer in the nPD-controller, called the *position and velocity observer*, based on (3). In order to obtain meaningful results in the comparison of different versions of τ_{BR}, it is important that the observer that provides the estimates of η and ν, as well as the nPD-controller are well tuned. Details about the tuning for position and velocity observer, the nPD-controller, and the bias compensation methods are presented in Section 4.4.

2.4.1. Method 1: Direct compensation

The first method we consider, common in the literature (Loría and Panteley, 1999), is to directly use the bias estimate from the position and velocity observer based on (3), tuned for good η and ν estimates, that is,

$$\tau_{BR} = R(\psi)^\top \hat{b}. \tag{5}$$

2.4.2. Method 2: Wave-filtered bias estimate

When we optimize the observer to work well for position and velocity in transients, we observe that the bias estimate is fast, but very oscillatory in steady state. This is elaborated in Section 4.2. By assumption, the bias load b from (3) is low-frequency, but for sufficiently high tuning of the observer (3) the bias estimate will oscillate due to wave-induced behavior. Therefore, we suggest to add an extra wave filter on the bias estimate before this is sent to the controller.

For this method we make the assumption that the bias load contains a wave-component in addition to the low-frequency part that we want to compensate. Accordingly, we redefine the bias load in (1c) to

$$b := b_{lf} + C_w b_w, \tag{6}$$

where $C_w b_w \in \mathbb{R}^3$ and $b_{lf} \in \mathbb{R}^3$ are the wave-frequency and low-frequency components of the bias load from (1c), respectively.

In the bias wave-filter we treat the bias estimate $\hat{b}$ from the observer (3) as the input to the filter and assume that:

(A2) The bias estimate $\hat{b}$ from (3c) is given as $\hat{b} := b_{lf} + C_w b_w$.

The model used for the bias dynamics has the same wave dynamics as in (3a), where

$$\dot{b}_w = A_w b_w + E_w w_{bw} \tag{7a}$$

$$\dot{b}_{lf} = 0 \tag{7b}$$

and the observer is given as

$$\dot{\hat{b}}_w = A_w \hat{b}_w + K_{b,1}(\omega_0)\tilde{b} \tag{8a}$$

$$\dot{\hat{b}}_{lf} = K_{b,2}\tilde{b} \tag{8b}$$

$$\hat{b}_2 = \hat{b}_{lf} + C_w \hat{b}_w \tag{8c}$$

where $\tilde{b} := \hat{b} - \hat{b}_2$. The low-frequency estimate of the bias is used in feedback, such that τ_{BR} is given as

$$\tau_{BR} = R(\psi)^\top \hat{b}_{lf}. \tag{9}$$

2.4.3. Method 3: Separate bias observer

The third bias compensation method is to use the bias estimate from a separate observer with the same structure as in (3), but with a tuning optimized to find a bias estimate that closely resembles the true low-frequency bias load.

Let us denote the estimate from this bias observer as $\hat{b}_{BO}$, and then τ_{BR} is given as

$$\tau_{BR} = R(\psi)^\top \hat{b}_{BO}. \tag{10}$$

2.4.4. Method 4: Integral action

The last method we consider is perhaps the most common choice for τ_{BR}, and that is integral action in the control law (Sørensen, 2011). A new integral state ζ is defined with dynamics

$$\dot{\zeta} = \hat{\eta} - \eta_d(t), \tag{11}$$

such that

$$\tau_{BR} = -K_i R(\psi)^\top \zeta. \tag{12}$$

2.5. Problem statement

We consider both the case where the bias b is slowly-varying for long periods of time, and also the case when b changes rapidly due to transient events. The objective is to compare the four different model-based approaches for τ_{BR} to compensate the bias loads, in order to gain insight on the efficiency of the methods and make conclusions on when the best overall closed-loop performance is obtained. The comparisons will be based on closed-loop key performance indicators (KPIs) that measure the low-frequency positioning performance and thrust utilization.

3. Setup and implementation

To test the different bias compensation methods, an SVM is used along with two different test maneuvers that include a combination of transients and longer periods of steady state.

3.1. Simulation verification model

The simulation model is a 6 DOF high-fidelity model of a platform supply vessel, with main parameters given in Table 1. The model is based on building blocks from the MSS Toolbox (Fossen and Perez, 2004), and includes Coriolis, centripetal forces, and linear and nonlinear damping; see Appendix A. To give a realistic load variation with heading angle of the vessel, lookup tables are used to calculate the loads acting on the vessel. The model is subject to waves from a sea state taken from the JONSWAP[1] spectrum, with a significant wave height of 6 m, and a peak frequency of 0.53 rad/s. The mean incident wave direction is 190° (head waves) in the North/East frame (Price and Bishop, 1974). The simulation also includes a current with a speed of 0.5 m/s and direction of 30°. The sensor models include realistic noise and sensor effects. The GPS is updated at 1 Hz, and the compass is updated at 10 Hz. The vessel is controlled by (4), which operates at 1 Hz. In addition, a first order lowpass thrust dynamics with a 5 s time constant is included.

[1] Joint North Sea Wave Project.

Table 1
Simulation, platform supply vessel, main parameters.

Parameters	Value
Length between perp.	80 m
Breadth	17.4 m
Draft	5.6 m
Displacement	6150 tons

3.2. Maneuvers

For the simulations presented in Section 5, two maneuvers are performed, both with the environmental conditions described in Section 3.1 above. One training maneuver, which is used to tune the observers and controller, and one test maneuver that uses the same tuning. This is to verify that the tuning is not an overfit to the training maneuver.

Both maneuvers are 1500 s in duration. For the training maneuver there is a combined North/East setpoint change and heading change of 90° at 300 s, and at 600 s there is a change of 45° in the direction of the current. The current direction changes as a first order filtered step response with time constant of 30 s. This is an exaggerated case, not necessarily very realistic, designed to challenge the algorithms. This gives three transient events for a short time frame, and about the last half of the maneuver, the conditions are steady, in order to compare the steady state performance as well. The test maneuver has a combined North/East setpoint and heading change at 300 s, where the heading changes 70°, and at 500 s there is also a combined setpoint and heading change with a heading change of 50°. Finally, at 800 s there is a pure heading change of 90°.

3.3. Closed-loop performance evaluation

To evaluate the closed-loop positioning performance of the algorithms, combinations of the following metrics are used,

$$J^c_{\tilde{\eta}} = \int_{t_0}^{t_f} \left\{ |\eta_N - \eta_{d,N}| + |\eta_E - \eta_{d,E}| + \frac{180}{\pi}|\psi - \psi_d| \right\} dt \tag{13a}$$

$$J^c_{\tau,uv} = \int_{t_0}^{t_f} \left\{ |\tau_{surge}| + |\tau_{sway}| dt \right. \tag{13b}$$

$$J^c_{\tau,r} = \int_{t_0}^{t_f} |\tau_{yaw}| dt, \tag{13c}$$

where the states and the elements of τ are defined in (1), and t_0 and t_f are the initial and final time of the interval. $J^c_{\tilde{\eta}}$ is a positioning performance metric, whereas $J^c_{\tau,uv}$ and $J^c_{\tau,r}$ are control effort metrics.

4. Tuning

In this section the tuning for the observers, nPD-controller and the bias compensation methods are presented. The maneuver used in the tuning is the training maneuver described in Section 3.2.

4.1. Derivative free optimization for tuning

In order to allow for a fair comparison of the bias compensation methods, optimization is used to find observer tuning. Classic optimization methods are not applicable due to a lack of information about the gradient, Hessian, or higher order derivatives. Thus, derivative free optimization (DFO) is used, specifically the MATLAB® function *fminsearch*.

To illustrate how DFO works, consider the example where we have one state variable $x \in \mathbb{R}$ where the objective is to minimize the error $\tilde{x} = x - \hat{x}$, and $\hat{x}$ is our state estimate. The observer has an injection gain $K \in \mathbb{R}$, and we select a cost function that depends on the injection gain and the time of the interval $J(K, t_{int})$, where $t_{int} = t_f - t_0$, and t_f and t_0 are the final and initial time of the interval. We initialize the DFO by selecting an initial guess for K, and the DFO evaluates the cost of J. Thereafter, the DFO algorithm selects values close to the initial K value to see if they provide a lower cost for J. It then selects the K that gave the lowest value and repeats the process. Note that the DFO can get stuck in a local minimum, so several runs with varying initial conditions have to be performed.

The different observer performance evaluations metrics used in this paper are

$$J_{\hat{\eta}} = \int_{t_0}^{t_f} \left\{ |\eta_N - \hat{\eta}_N| + |\eta_E - \hat{\eta}_E| + \frac{180}{\pi}|\psi - \hat{\psi}| \right\} dt \tag{14a}$$

$$J_{\hat{\nu}} = \int_{t_0}^{t_f} \left\{ |u - \hat{u}| + |v - \hat{v}| + \frac{180}{\pi}|r - \hat{r}| \right\} dt \tag{14b}$$

$$J_{\hat{b}_N} = \int_{t_0}^{t_f} |b_N - \hat{b}_N| dt \tag{14c}$$

$$J_{\hat{b}_E} = \int_{t_0}^{t_f} |b_E - \hat{b}_E| dt \tag{14d}$$

$$J_{\hat{b}_\psi} = \int_{t_0}^{t_f} |b_\psi - \hat{b}_\psi| dt, \tag{14e}$$

where the states are defined in (1) and the estimates in (3).

4.2. Tuning of position and velocity observer

The injection gains K_1 and K_2 in (3) for the wave and η-dynamics are found by the tuning rules proposed by Fossen and Strand (1999), which give good wave-filtering. The tuning for K_3 and K_4 is optimized for finding good η and ν estimates, and is found by derivative free optimization. The corresponding cost function J used in the DFO is then

$$J = J_{\hat{\eta}} + c_\nu J_{\hat{\nu}}, \tag{15}$$

where $J_{\hat{\eta}}$ and $J_{\hat{\nu}}$ are given by (14a) and (14b), and $c_\nu \in \mathbb{R}_{>0}$ is a scaling parameter set such that the contributions from the velocity estimation error $c_\nu J_{\hat{\nu}}$ and the position estimation errors are balanced. The value we used was $c_\nu = 7$. The vessel is controlled by (4) using state estimates together with the integral action (11)–(12). The tuning of the observer is found in several iterations, and for each iteration the observer tuning is updated with the resulting DFO tuning from the previous run. Thereafter, a new closed-loop run was performed, serving as the dataset of the next round of DFO runs, until the observer tuning converged.

The resulting bias estimate from the observer tuned with (15), along with the actual bias load found by solving for b in (1d), are shown in Fig. 1. Note that the bias estimate tracks the actual mean bias load well, but since the bias estimation is not part of the evaluation function (15) it is quite oscillatory in steady state.

4.3. nPD-controller tuning

The tuning for the nonlinear PD-controller is given by the tuning rules outlined in Fossen (2011) by specifying desired eigenfrequencies and damping ratios of the response, as if the system is linear, that is, by setting the rotation matrix to identity. Thereafter, the tuning is adjusted through trial and error using the well-tuned η and ν estimates from the position and velocity observer.

4.4. Tuning of the bias compensation methods

4.4.1. Tuning method 1: direct compensation

The tuning of Method 1 is given by the tuning of the position and velocity observer as outlined in Section 4.2. No further tuning is needed.

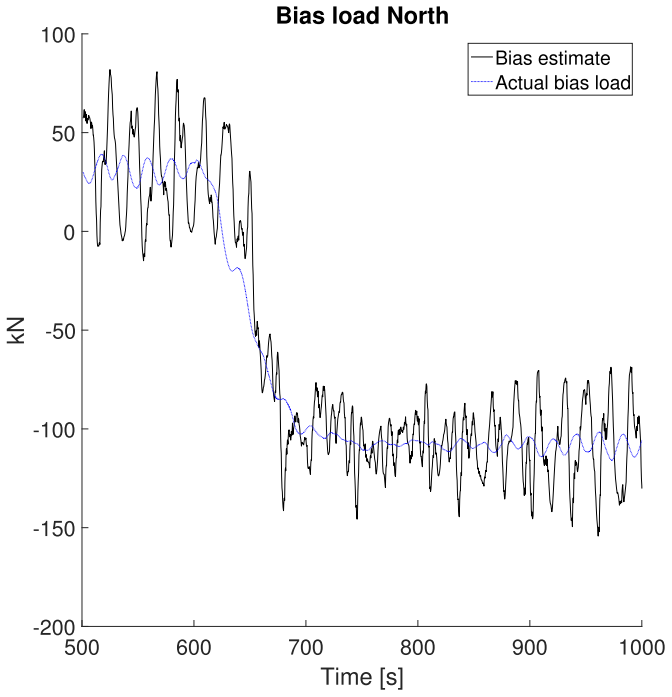

Fig. 1. Bias estimate from the position and velocity observer and the true bias load in the North direction.

4.4.2. Tuning method 2: wave-filtered bias estimate

Method 2 uses the bias estimate $\hat{b}$ from the position and velocity observer in Section 4.2 as input, that is, the bias estimate used in Method 1. The tuning of the matrices K_{b1} and K_{b2} in the wave filter of (8) are found by the tuning rules proposed by Fossen and Strand (1999). That is, K_{b1} and K_{b2} are similar to K_1 and K_2 in (3), respectively.

4.4.3. Tuning method 3: bias observer

For Method 3 the cost function J_{BO} used in the DFO is

$$J_{BO} = c_{b_N} J_{\hat{b}_E} + c_{b_E} J_{\hat{b}_N} + c_{b_\psi} J_{\hat{b}_\psi} \tag{16}$$

where $J_{\hat{b}_N}$, $J_{\hat{b}_E}$, and $J_{\hat{b}_\psi}$ are given by (14c)-(14e), and c_{b_N}, c_{b_E}, $c_{b_\psi} \in \mathbb{R}_{>0}$ are scaling parameters to balance the contributions from the three bias terms. The values used were $c_{b_N} = 0.587$, $c_{b_E} = 1$, and $c_{b_\psi} = 0.055$. This is to make the observer equally responsive to all the three bias forces. For instance, in the training dataset, the North bias force is larger than the East bias force over the maneuver. An equal weighting with $c_{b_N} = c_{b_E}$ would have made the observer more aggressive in observing the North bias. With the chosen weights this is avoided. The DFO tuning process is similar to that of Section 4.2.

4.4.4. Tuning method 4: integral action

For Method 4 the tuning for K_i in (12) was found through extensive trial and error, starting at the tuning given in Fossen (2011). In the following we provide a reasonable documentation for a good K_i-tuning, where it is shown that K_i-values above and below the chosen tuning are less optimal. To document the choice of a good K_i−tuning the cost function $J_{\tilde{\eta}}^c$ from (13a) is shown for several values of K_i in Table 2, applied on the maneuver described in Section 3.2 as the main maneuver. The different values for K_i in Table 2 are given as $K_{i,j} = \rho_j K_{i1}$, $j = 1, ...,5$, where ρ_j, $j = 1, ...,5$ are positive scalars that satisfy $\rho_{j+1} > \rho_j$, $j = 1, ...,4$. The results of the table clearly show that K_{i3} gives the minimum value, and the lower and higher values of K_i give less optimal performance.

Table 2
Results for the integral action tuning on the training maneuver. The table shows the KPI in (13a). The KPIs are normalized such that the worst performing has a value of maximum of 100 for the whole maneuver.

Step	$K_i\,[10^5]$	$J_{\tilde{\eta}}^c$
1	diag{0.0132, 0.0115, 6.314}	99.88
2	diag{0.0142, 0.0123, 6.765}	99.59
3	diag{0.0151, 0.0131, 7.188}	99.58
4	diag{0.0160, 0.0139, 7.6673}	99.74
5	diag{0.0170, 0.0148, 8.1183}	100.00

Table 3
Summary of the bias compensation methods.

Method	Description
1	Direct comp. from pos/vel observer
2	Wave-filtered bias compensation
3	Comp. from separate bias observer
4	Integral action

5. Results and discussion

5.1. Simulation results

Results for the four different bias rejection methods are presented in the following. See Table 3 for a summary of the methods. The vessel performs the two different maneuvers presented in Section 3.2. The results on the training maneuver are shown in Fig. 2, Fig. 5, and Table 4. Fig. 2 has three plots. The upper left plot shows the low-frequency position and heading for the run with Method 1. The lower left plot shows the different bias rejection terms in surge only, and the right plot shows the cumulative error $J_{\tilde{\eta}}^c$ of the positioning performance from (13a). Table 4 shows all the performance indices from (13) both for the whole maneuver and also for the steady-state time interval from 1000 to 1500 s. Fig. 5 shows the thrust KPIs $J_{\tau,uv}^c$ in (13b) and $J_{\tau,r}^c$ in (13c) for the training maneuver and the test maneuver.

The results for the training maneuver show that Method 3 (the bias observer) has the best overall performance. It is both fast over transients and calm in steady state. As seen from Table 4 and from Fig. 5, the thrust effort of Methods 3 and 4 are about equal, and lower than Methods 1 and 2, which also are approximately equal. During the steady period, the thrust effort of all four methods are similar, but Methods 3 and 4 have a lower positioning error than Methods 1 and 2.

Fig. 3 shows the bias rejection terms in surge for the four different methods in the upper plot. This is the same as the lower left plot of Fig. 2 zooming in on the transient at 600 s. The lower plot of Fig. 3 shows the difference between τ_{BR} and true bias force for the different methods for the respective simulations. As observed from Fig. 3, all four methods are quite fast in the transient, with Method 4 as the slowest. In steady state Method 4 is very calm, while Methods 2 and 3 are much calmer than Method 1.

As observed, Methods 1 and 2 have similar closed-loop performance. Even though Method 2 has smaller oscillations than Method 1, it also has a slight lag due to the extra filter, as observed from Fig. 3. The lag seems to make Method 2 underperform Method 1 during transients, and the two effects (lower oscillations and added lag) cancel in steady state, making the two methods similar in their steady-state performance. Method 3 has a good balance between steady-state and transient performance, and therefore has a better overall performance compared to Methods 1 and 2.

The results for the test maneuver is shown in Fig. 4, Fig. 5, and Table 5. The tuning used for the observers and controllers are the same as those used for the training maneuver. Similar type of results are seen. In the test maneuver there are more transient events and less steady

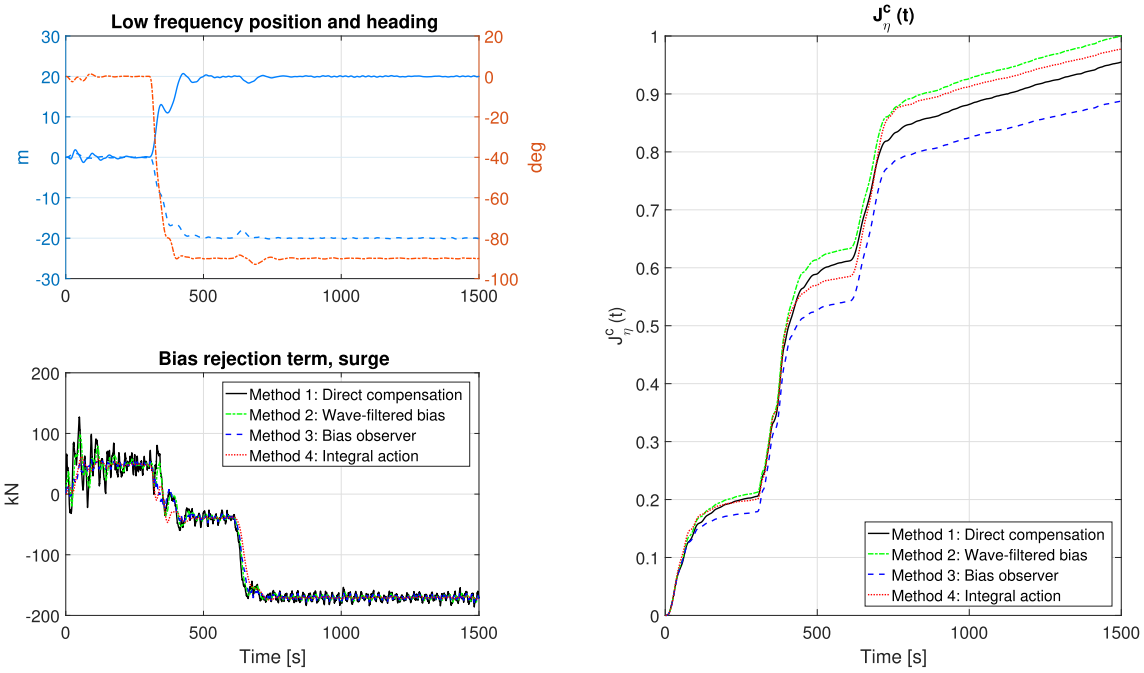

Fig. 2. Results for the four different bias rejection methods for the training maneuver. The right plot shows the KPI in (13a). The KPI is normalized such that the worst performing has a maximum of 1 for the whole maneuver.

Table 4
Results for the training maneuver. The table shows the KPIs from (13). The KPIs are normalized such that the worst performing has a value of maximum 100 (for the whole maneuver). The time interval 1000–1500 s is in steady state.

Time:	0–1500 s			1000–1500 s		
Controller	J^c_η	$J^c_{\tau,uv}$	$J_{\tau,r}$	J^c_η	$J^c_{\tau,uv}$	$J_{\tau,r}$
Method 1	95.5	100.0	99.5	7.3	42.4	29.6
Method 2	100.0	99.1	100.0	7.3	42.4	29.6
Method 3	88.8	97.5	98.7	6.3	42.4	29.6
Method 4	97.8	97.7	98.9	6.5	42.4	29.6

state than in the training maneuver. That is why Method 4 performs worse overall (in positioning performance) than in the training maneuver. However, note that Method 4 has the lowest thrust consumption. Method 3 still performs best, and Method 4 has the best steady-state behavior, and Method 3 has close to the same steady-state performance. This shows that the same tuning and observations also apply well for the test maneuver.

5.2. General discussion

The findings presented in Section 5.1 justify that using a bias estimate from a separate bias observer, with tuning optimized to estimate the bias, is the best way of compensating the bias loads in DP. This is better than the traditional integral action based on the tracking errors, since it mainly outperforms the integral action in transients. In addition, the results show that using the bias estimate (in feedback) from a single observer optimized for position and velocity estimates underperforms compared to using the separate bias observer both in transients and in steady state. The wave-filtered version of this bias estimate (from the position and velocity observer) underperforms the non-wave-filtered version, seemingly due to the added phase lag from the extra wave-filter. Using a separate bias observer is the best option among those presented in the paper. Direct integral action and bias compensation from the single position/velocity/bias observer have similar performance. If there are longer periods of steady state conditions,

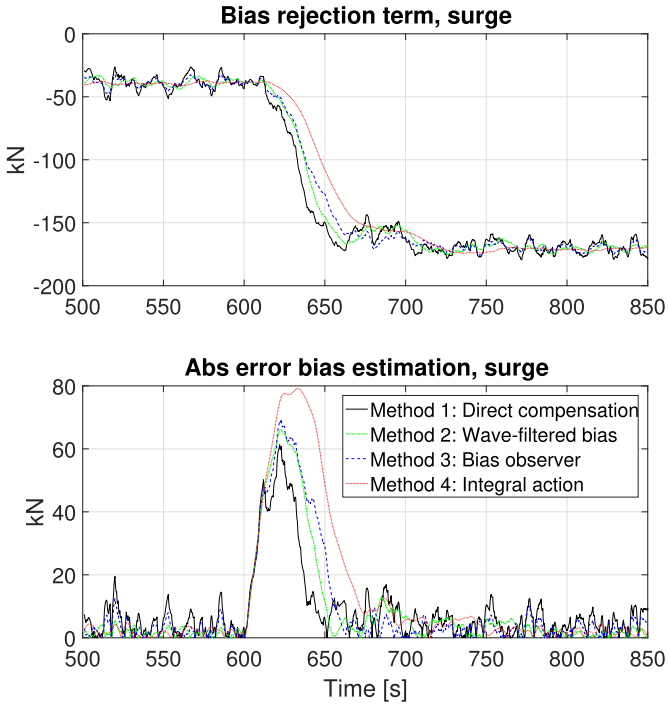

Fig. 3. The top plot shows the bias rejection term in surge for the four different methods on the training maneuver. The bottom plot shows the error between τ_{BR} and the true bias in surge (absolute value).

integral action is better than the single observer bias compensation, and vice versa for transient conditions.

6. Conclusion

In this paper, four methods for compensating the mean and slowly varying environmental loads (and unmodeled dynamics) for DP of marine vessels have been investigated. A high-fidelity simulation model

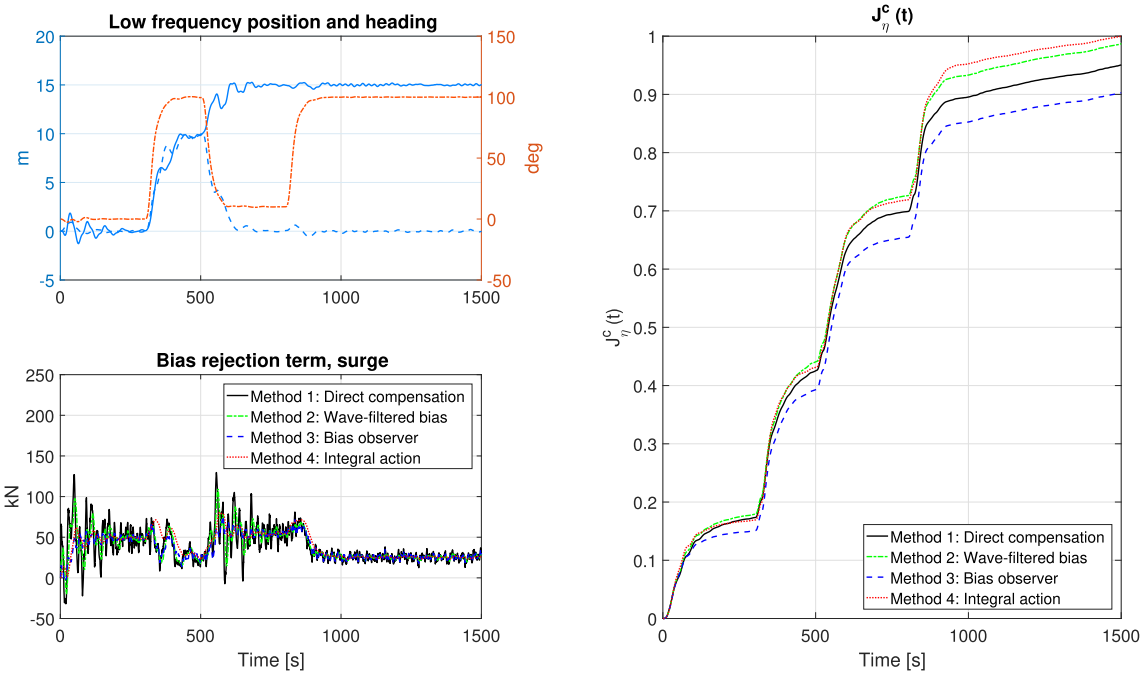

Fig. 4. Results for the four different bias rejection methods, on the test maneuver. The right plot shows the KPI in (13a). The KPI is normalized such that the worst performing has a maximum of 1 for the whole maneuver.

was used to compare the methods, using two different maneuvers; one training maneuver for tuning and one test maneuver for verification. All methods were tuned to work well for the training maneuver. Then this tuning was applied for the test maneuver to verify the gains, and similar performances were shown. The standard integral action was compared to three variations of using the bias estimate from a model-based observer. The results indicated that the best method to compensate the bias loads was using the bias estimate from a separate bias observer, for which the tuning was optimized to estimate the bias loads. This method displayed both the best transient and steady state behavior given the maneuvers in this paper.

Table 5
Results for the test maneuver. The table shows the KPIs from (13). The KPIs are normalized such that the worst performing has a value of maximum 100 (for the whole maneuver). The time interval 1000–1500 s is in steady state.

Time:	0–1500 s			1000–1500 s		
Controller	J^c_η	$J^c_{\tau,uv}$	$J_{\tau,r}$	J^c_η	$J^c_{\tau,uv}$	$J_{\tau,r}$
Method 1	95.1	100.0	99.4	5.5	24.3	24.4
Method 2	98.7	94.2	99.4	5.4	22.1	24.4
Method 3	90.3	92.0	99.5	5.0	22.0	24.4
Method 4	100.0	90.5	100.0	4.7	21.3	24.3

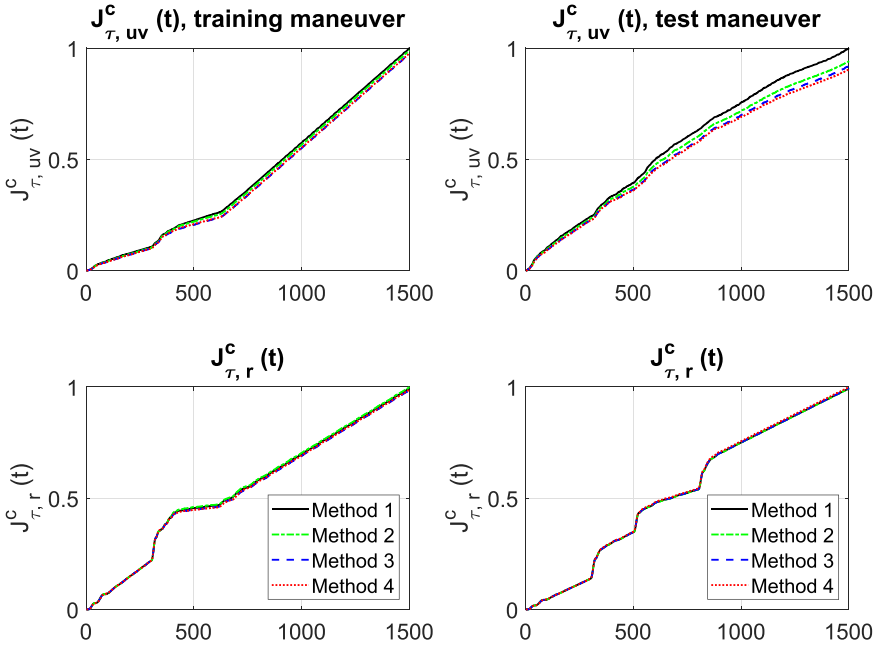

Fig. 5. Cumulative thrust results for the four different bias rejection methods, on the training maneuver (left) and the test maneuver (right). The top plots show the KPI in (13b) and the bottom plots show the KPI in (13c). The KPIs are normalized such that the worst performing has a maximum of 1 for the whole maneuver.

Acknowledgements

This work was supported by the Research Council of Norway, partly through the Centre of Excellence NTNU AMOS, project no. 223254, and partly through Centre for Research-based Innovation MOVE, project no. 237929. The authors would like to thank Vincenzo Calabrò from Norwegian Subsea for helpful discussion and input.

Appendix. Simulation verification model

The kinetics used in the SVM of the supply vessel, see Section 3.1, is (Sørensen, 2013)

$$M\dot{\nu} + C_{RB}(\nu)\nu + C_A(\nu_r)\nu_r + D_L\nu + d_{NL}(\nu_r) + G\eta = \tau + \tau_{env}, \tag{17}$$

where $M \in \mathbb{R}^{6\times6}$ is the inertia matrix, $C_{RB}(\nu) \in \mathbb{R}^{6\times6}$ and $C_A(\nu_r) \in \mathbb{R}^{6\times6}$ are the rigid body and added mass Coriolis matrices, respectively, $\nu \in \mathbb{R}^6$ and $\nu_r \in \mathbb{R}^6$ are the velocity and relative velocity, respectively, $D_L \in \mathbb{R}^{6\times6}$ is the linear damping matrix, $d_{NL}(\nu_r) \in \mathbb{R}^6$ is the non-linear damping vector, $G \in \mathbb{R}^{6\times6}$ is the restoring matrix, $\tau \in \mathbb{R}^6$ is the thrust vector, and $\tau_{env} \in \mathbb{R}^6$ is the environmental load vector. The inertia matrix for the SVM is a sum of the rigid body mass and the added mass, $M := M_{RB} + M_A$,

$$M_{RB} = \begin{bmatrix} mI_{3\times3} & -mS(r_g^b) \\ mS(r_g^b) & I_b \end{bmatrix}$$
$$= 10^8 \cdot \begin{bmatrix} 0.0615 & 0 & 0 & 0 & -0.3198 & 0 \\ 0 & 0.0615 & 0 & 0.3198 & 0 & -0.1414 \\ 0 & 0 & 0.0615 & 0 & 0.1414 & 0 \\ 0 & 0.3198 & 0 & 31.4290 & 0 & -0.7355 \\ -0.3198 & 0 & 0.1414 & 0 & 4.2767 & 0 \\ 0 & -0.1414 & 0 & -0.7355 & 0 & 16.6653 \end{bmatrix} \tag{18}$$

$$M_A = 10^8 \cdot \begin{bmatrix} 0.0053 & 0 & -0.0036 & 0 & -0.7101 & 0 \\ 0 & 0.0518 & 0 & 0.1135 & 0 & 0.0095 \\ -0.0036 & 0 & 0.1993 & 0 & 1.9683 & 0 \\ 0 & 0.1128 & 0 & 2.6167 & 0 & -1.9025 \\ -0.7070 & 0 & 1.9664 & 0 & 177.7000 & 0 \\ 0 & 0.0095 & 0 & -1.9082 & 0 & 15.2660 \end{bmatrix} \tag{19}$$

where m is the mass of the ship, here $m = 6150$ tons, and $I_b := I_g - mS^2(r_g^b)$, where I_g is the inertia matrix about the body's center of gravity, $r_g^b = \mathrm{col}(-2.3m, 0, -5.2m)$. The matrix $S(\lambda)$, where $\lambda = \mathrm{col}(\lambda_1, \lambda_2, \lambda_3) \in \mathbb{R}^3$, denotes a skew-symmetric matrix,

$$S(\lambda) = \begin{bmatrix} 0 & -\lambda_3 & \lambda_2 \\ \lambda_3 & 0 & -\lambda_1 \\ -\lambda_2 & \lambda_1 & 0 \end{bmatrix}. \tag{20}$$

The rigid body and added mass Coriolis matrices are calculated online during simulations from the inertia matrices M_{RB} and M_A given above, and the velocity ν and relative velocity ν_r. The rigid body Coriolis can be written as Fossen (2011):

$$C_{RB}(\nu) = \begin{bmatrix} 0_{3\times3} & -mS(\nu_1) - mS(\nu_2)S(r_g^b) \\ -mS(\nu_1) + mS(r_g^b)S(\nu_2) & -S(I_b\nu_2) \end{bmatrix}, \tag{21}$$

where the linear and angular velocities are written as $\nu_1 = \mathrm{col}(u, v, w)$, $\nu_2 = \mathrm{col}(p, q, r)$. The added mass Coriolis is calculated in a similar way, see Sørensen (2013) for a complete representation. The nonlinear damping is calculated from a look-up table. The linear damping matrix D_L, and restoring force matrix G are

$$D_L = 10^8 \cdot \begin{bmatrix} 0.0017 & 0 & 0 & 0 & -0.0115 & 0 \\ 0 & 0.0014 & 0 & 0.0147 & 0 & -0.0065 \\ 0 & 0 & 0.0387 & 0 & 0.0891 & 0 \\ 0 & 0.0147 & 0 & 1.6800 & 0 & -0.0338 \\ -0.0115 & 0 & 0.0891 & 0 & 16.5299 & 0 \\ 0 & -0.0065 & 0 & -0.0338 & 0 & 0.6386 \end{bmatrix}$$

$$G = 10^9 \cdot \begin{bmatrix} 0 & 0 & 0 & 0 & 0 & 0 \\ 0 & 0 & 0 & 0 & 0 & 0 \\ 0 & 0 & 0.0141 & 0 & 0.0324 & 0 \\ 0 & 0 & 0 & 0.1931 & 0 & 0 \\ 0 & 0 & 0.0324 & 0 & 4.2977 & 0 \\ 0 & 0 & 0 & 0 & 0 & 0 \end{bmatrix}.$$

References

Balchen, J.G., Jenssen, N.A., Sælid, S., 1976. Dynamic positioning using kalman filtering and optimal control theory. IFAC/IFIP symposium on automation in offshore oil field operation 183, 186.

Blanke, M., Kinnaert, M., Lunze, J., Staroswiecki, M., 2003. Diagnosis and Fault-Tolerant Control. Springer.

Brodtkorb, A.H., Værnø, S.A., Teel, A.R., Sørensen, A.J., Skjetne, R., 2016. Hybrid observer for improved transient performance of a marine vessel in dynamic positioning. In: Proceedings of the IFAC Symposium on Nonlinear Control Systems 2016, vol. 49. pp. 345–350 (18).

Brodtkorb, A.H., Værnø, S.A., Teel, A.R., Sørensen, A.J., Skjetne, R., 2018. Hybrid controller concept for dynamic positioning of marine vessels with experimental results. Automatica 93, 489–497.

Du, J., Hu, X., Liu, H., Chen, C.P., 2015. Adaptive robust output feedback control for a marine dynamic positioning system based on a high-gain observer. IEEE Trans. Neural Netw. Learning Syst. 26 (11), 2775–2786.

Fossen, T.I., 2011. Handbook of Marine Craft Hydrodynamics and Motion Control. John Wiley & Sons.
Fossen, T.I., Perez, T., 2004. Marine Systems Simulator (Mss). https://github.com/cybergalactic/MSS, Accessed date: 24 February 2017.
Fossen, T.I., Perez, T., 2009. Kalman filtering for positioning and heading control of ships and offshore rigs. IEEE Control Syst. Mag. 29 (6), 32–46.
Fossen, T.I., Strand, J.P., 1999. Passive nonlinear observer design for ships using lyapunov methods: full-scale experiments with a supply vessel. Automatica 35 (1), 3–16.
Kjerstad, Ø.K., Skjetne, R., 2016. Disturbance rejection by acceleration feedforward for marine surface vessels. IEEE Access 4, 2656–2669.
Lindegaard, K.-P., 2003. Acceleration Feedback in Dynamic Positioning. PhD thesis. Norwegian University of Science and Technology, Trondheim, Norway.
Loria, A., Fossen, T.I., Panteley, E., 2000. A separation principle for dynamic positioning of ships: theoretical and experimental results. IEEE Trans. Control Syst. Technol. 8 (2), 332–343.
Loría, A., Panteley, E., 1999. A Separation Principle for a Class of Euler-Lagrange Systems, New Directions In Nonlinear Observer Design. Springer, pp. 229–247.
Perez, T., 2009. Anti-wind-up designs for dynamic positioning of marine vehicles with control allocation. IFAC Proceedings Volumes 42 (18), 243–248.
Price, W.G., Bishop, R.E.D., 1974. Probabilistic Theory of Ship Dynamics. Halsted Press.
Refsnes, J.E., Sørensen, A.J., 2007. Comparison of two observers for marine vessels in ocean current. IFAC Proceedings Volumes 40 (17), 32–37.
Sørensen, A.J., 2011. A survey of dynamic positioning control systems. Annu. Rev. Contr. 35 (1), 123–136.
Sørensen, A.J., 2013. Marine Control Systems - Lecture Notes. Department of Marine Technology, Norwegian Univ. of Sci. and Tech.
Tannuri, E.A., Morishita, H.M., 2006. Experimental and numerical evaluation of a typical dynamic positioning system. Appl. Ocean Res. 28 (2), 133–146.
Værnø, S.A., Brodtkorb, A.H., Skjetne, R., Calabrò, V., 2017. Time-varying Model-Based Observer for Marine Surface Vessels in Dynamic Positioning. IEEE Access.
Værnø, S.A., Brodtkorb, A.H., Skjetne, R., Sørensen, A.J., 2016. An output feedback controller with improved transient response of marine vessels in dynamic positioning. In: Proceedings of the IFAC Conference on Control Applications in Marine Systems 2016, vol. 49. pp. 133–138 (23).
Værnø, S.A., Skjetne, R., Kjerstad, Ø.K., Calabrò, V., 2019. Comparison of control design models and observers for dynamic positioning of surface vessels. Contr. Eng. Pract. 85, 235–245.